Combined 6-DoF motion tracking and photogrammetry to capture drag anchor installation behaviour in sand

J. Fan
Centre for Offshore Foundation Systems (COFS), The University of Western Australia, Perth, Australia, junhao.fan@research.uwa.edu.au

B. Ferrell, C. D. O'Loughlin, M. F. Bransby, P. G. Watson
Centre for Offshore Foundation Systems (COFS), The University of Western Australia, Perth, Australia benjamin.ferrell@uwa.edu.au, conleth.oloughlin@uwa.edu.au, fraser.bransby@uwa.edu.au, phillip.watson@uwa.edu.au

ABSTRACT: Accurate observations of drag embedment anchor installation remain challenging because anchor motion and soil deformation occur beneath the soil surface. This study presents a coupled measurement system that integrates six-degree-of-freedom (6-DoF) optical marker tracking with photogrammetric reconstruction of the sand surface, enabling quantitative assessment of anchor kinematics and soil response during installation. Preliminary 1g dry-sand tests using a 1:80-scale anchor model are reported in this paper to verify the system's reliability, with Ng tests planned for the near future. The 6-DoF system accurately resolved anchor position and orientation, while photogrammetry captured the progressive soil deformation during installation. The combined results reveal a clear correlation between the anchor position and the shape of the soil surface, demonstrating the method's ability to visualise and quantify anchor-soil interaction. This novel experimental set-up provides a practical tool for future centrifuge model tests and can be readily extended to other geotechnical tests such as piles, plate anchors, and pipelines.

1 INTRODUCTION

Drag embedment anchors are widely recognised as an efficient and cost-effective solution for mooring floating offshore structures. In a typical installation, the anchor is first positioned on the seabed at a predetermined location and then dragged horizontally by an Anchor Handling Vessel (AHV) until either the design load is reached or the vessel capacity is mobilised. While the final anchor location is usually specified in a mooring analysis, in practice it is difficult to determine the exact position once the anchor becomes fully buried beneath the seabed. A clear understanding of the installation behaviour of drag anchors is therefore essential for improving predictive models and validating design methodologies. Such understanding relies on physical modelling supported by reliable measurement techniques. However, anchor motion and soil–structure interaction are concealed within the soil, posing significant challenges to direct observation.

Over the past decades, various approaches have been developed to overcome this limitation. Early studies by LeLievre et al. (1981) and Neubecker et al. (1996) employed plane-strain tests in glass-sided tanks to directly observe soil deformation and anchor rotation. These tests successfully revealed key failure mechanisms but constrained lateral soil movement, leading to differences from true three-dimensional behaviour. To enable 3D tracking, Carchedi et al. (1984) designed a potentiometer-based tracking system that measured the length variations of three lines connected to the anchor shank, enabling calculation of its location and rotation. Neubecker (1996) also introduced a tracking probe method for 3D model tests, in which an aluminium rod was attached to the anchor shank and extended above the soil surface, enabling video-based visual measurements of the anchor's drag distance, pitch angle, and penetration depth during installation. However, this method is unable to capture the anchor's roll and yaw rotations, limiting its capability to fully resolve six-degree-of-freedom (6-DoF) motion. Subsequent developments incorporated embedded sensors. For instance, Liu et al. (2010) employed two tilt sensors to monitor pitch and roll, while Gerkus et al. (2019) proposed a magnetometer-based tracking system capable of real-time 6-DoF tracking – although for the latter, magnetic interference from strongbox walls could distort the magnetic field and restrict the effective testing area (Shu et al., 2022). More recently, Sharif et al. (2025) developed a wireless inertial-measurement-unit tracking system, in which the anchor's penetration depth was obtained by integrating orientation-corrected acceleration data using a Kalman filter. This was demonstrated to be successful in centrifuge model tests in dry sand, but as noted in Sharif et al. (2025), would not work in its current form in saturated soil samples and would require a higher battery capacity to allow for the longer logging duration in tests where the anchor may need to be dragged at a slower rate to achieve a different drainage response.

To address the limitations outlined above, an image-based measurement system was developed that is capable of resolving both anchor kinematics and soil-surface deformation during an anchor installation. The system integrates optical tracking and photogrammetry to obtain datasets of anchor motion and soil surface response. This paper presents the design and validation of the system through preliminary 1g dry-sand tests on a scaled STEVSHARK® MK5 anchor, and illustrates how the combined data can be visualised to interpret key mechanisms occurring during anchor installation. The system provides a practical basis for future centrifuge modelling of drag embedment anchors and of other infrastructure involving large deformations.

2 EXPERIMENTAL METHODOLOGY

To verify the measurement accuracy and visualisation capability of the proposed system, a set of anchor installation tests was performed at 1g in dry sand. Details of these experiments are provided in the following sections.

2.1 Overview of experimental arrangement

A uniformly graded fine silica sand was air pluviated into a strongbox measuring 650 mm × 390 mm × 325 mm (length × width × depth). The sample was then vacuum levelled to create a flat soil surface, resulting in a sample of depth 250 mm. A medium-dense condition was achieved with a dry unit weight of 16.8 kN/m^3 (relative density, $D_r \approx 67\%$).

The STEVSHARK® MK5 (20 t) drag anchor (Vryhof, 2018), a widely used commercial design, was selected as the prototype for this testing. A 1:80 scale model (to accommodate future 80g centrifuge testing) was fabricated by 3D metal printing in aluminium to ensure geometric accuracy. Although the prototype fluke is hollow, fabrication constraints required a solid model; aluminium was therefore adopted to achieve the correct model-scale mass (35.8 g for a volume of 12,270 mm^3, corresponding to approximately 20 t at prototype scale). The configuration and principal dimensions are shown in Figure 1(a).

To drag the anchor into the sand, an actuator–pulley system was used. The anchor model was connected to a load cell mounted on the actuator through two pulleys using a 1.5 mm thick Dyneema® rope. The lower pulley was attached to the actuator frame and positioned at the sand surface to maintain a zero-degree uplift angle, while the upper pulley was mounted on a motor-driven vertical carriage. Owing to the 2:1 pulley arrangement, the anchor experienced twice the displacement of the carriage.

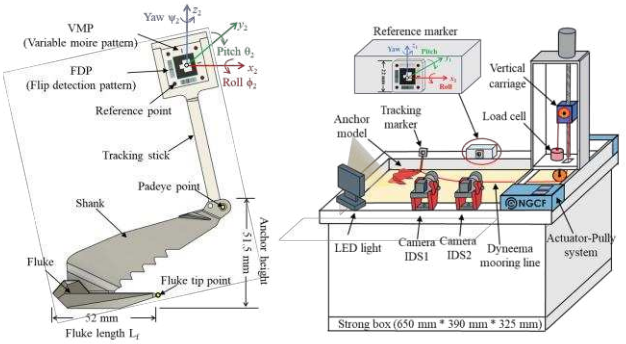

(a) (b)

Figure 1. Drag anchor experiments: (a) anchor model with marker, (b) experimental arrangement

2.2 6-DoF marker tracking system

To record the anchor trajectory and quantify its 6-DoF behaviour during installation, an optical marker-tracking system was employed.

2.2.1 Marker tracking device

As shown in Figure 1(b), the tracking system consisted of two IDS machine vision cameras (model GV-5270CP-C-HQ), a light source, and bespoke Photron 6D markers. The cameras operated at a resolution of 2048 × 1536 pixels and a frame rate of 10 fps. The images were processed using the proprietary Photron 6D-Marker Analyst software to identify the markers and determine their motion. To establish a spatial reference for motion tracking, two markers were used: a reference marker defining the coordinate system and a tracking marker measuring the position and orientation of the moving object. The reference marker was fixed at a predetermined position on the strongbox, whereas the tracking marker was located on the end of a tracking stick which was made of PLA and extended from the anchor (see Figure 1(a)). Each marker measured 22 mm × 22 mm × 2.35 mm (length × width × thickness). The tracking stick had a streamlined shape to minimise soil disturbance, with a total mass of 3.7 g (including the mass of the marker), which is low relative to the mass of the anchor (35.8 g).

Once installed, the tracking system determined the 6-DoF position of the marker by recognising the optical patterns. As shown in Figure 1(a), each marker contains four reference points at its corners to define the translational coordinates (x, y, and z). The flip detection pattern and variable moiré pattern, which vary with viewing angle, are used to measure the marker's orientation angles (roll, pitch, yaw). During installation, images were captured continuously, and the software processed these images to compute the 6-DoF motions of each marker.

2.2.2 Analysis of marker tracking data

The software provided the three-dimensional position (*x, y,* and *z*) and orientation (roll, pitch, and yaw) of the tracking marker's centre. Since the marker was fixed to the anchor, its measured motion represents that of the entire anchor body. The motion of any point on the anchor can therefore be described by a rigid-body transformation relating the local and global coordinate systems, as

$$P_{global} = RP_{local} + d \tag{1}$$

where $P_{local} = [x_2, y_2, z_2]^T$ is the position vector of a point on the anchor expressed in the local coordinate system fixed to the tracking marker, R is the 3 × 3 rotation matrix defining the tracking marker's orientation relative to the global coordinate axes, and $d = \left[d_{x1}, d_{y1}, d_{z1}\right]^T$ is the translation vector representing the position of the marker's centre in the global (reference-marker-based) coordinate system. The transformed vector $P_{global} = [x_1, y_1, z_1]^T$ thus represents the global position of the same point after applying rotation and translation relative to the reference marker.

The rotation matrix R followed the right-hand rule and was expressed as the product of three sequential rotations about the *x*-, *y*-, and *z*-axes, namely roll (ϕ_2), pitch (θ_2), and yaw (ψ_2):

$$R = R_z(\psi_2) \cdot R_y(\theta_2) \cdot R_x(\phi_2) \tag{2}$$

where $R_x(\phi_2)$, $R_y(\theta_2)$ and $R_z(\psi_2)$ are the elemental rotation matrices, defined as follows:

$$R_x(\phi_2) = \begin{bmatrix} 1 & 0 & 0 \\ 0 & \cos\phi_2 & -\sin\phi_2 \\ 0 & \sin\phi_2 & \cos\phi_2 \end{bmatrix} \tag{3}$$

$$R_y(\theta_2) = \begin{bmatrix} \cos\theta_2 & 0 & \sin\theta_2 \\ 0 & 1 & 0 \\ -\sin\theta_2 & 0 & \cos\theta_2 \end{bmatrix} \tag{4}$$

$$R_z(\psi_2) = \begin{bmatrix} \cos\psi_2 & -\sin\psi_2 & 0 \\ \sin\psi_2 & \cos\psi_2 & 0 \\ 0 & 0 & 1 \end{bmatrix} \tag{5}$$

Based on the above transformation, the global coordinates of any point on the anchor can be obtained from the 6-DoF tracking data.

2.2.3 Verification of marker accuracy

The positional and angular accuracies of the optical tracking system were evaluated using a specifically-designed 3D-printed calibration plate (Figure 2) with predefined slots corresponding to each translational (*x*, *y*, *z*) and rotational (roll, pitch, yaw) degree of freedom. The 160 × 110 mm plate was fabricated using a Bambu Lab X1 Carbon printer with a typical positional accuracy of about ±0.1 mm, ensuring negligible fabrication errors relative to the measurement uncertainty. During calibration, the marker was sequentially placed in each slot, and its measured displacements and rotations were compared with the reference positions to obtain the root-mean-square (RMS) errors. The system achieved translational accuracies of 0.1 mm, 1.4 mm, and 0.3 mm in the *x*, *y*, and *z* directions and rotational accuracies of 0.8°, 0.3°, and 0.1° for roll, pitch, and yaw, respectively. These results confirm sub-millimetre and sub-degree precision, demonstrating that the tracking system provides adequate accuracy for the tests relative to the anchor size.

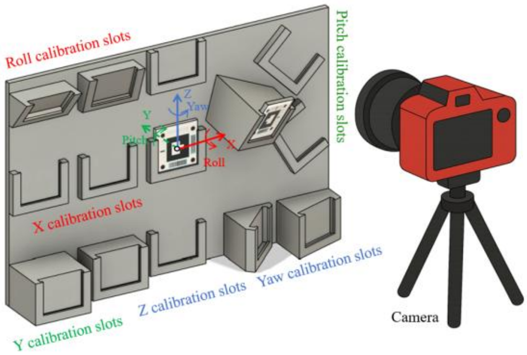

Figure 2. Marker accuracy verification tests

2.3 Photogrammetric soil reconstruction

To investigate the soil deformation and anchor–soil interaction, the position of the sand surface was reconstructed using photogrammetry. Short videos were recorded from multiple viewing angles above the sand surface to fully capture the geometry of the deformed sand surface. To ensure correct scaling and verify reconstruction accuracy, two metal blocks of different sizes were placed near the anchor trajectory for calibration. The recorded videos were processed using Polycam, a photogrammetry software that automatically extracted overlapping frames and reconstructed a 3D point cloud of the sand surface.

The dense point cloud was exported as an *.obj* file containing the spatial coordinates (*x, y, z*) of surface points and their triangulated mesh connections. The model was subsequently imported into ParaView for post-processing. One calibration block was used to scale the model to real dimensions, while the other was used to assess the measurement accuracy, resulting in an RMS error of 0.46 mm. To facilitate quantitative interpretation, surface clipping and sectional slicing were then applied to isolate the region of interest, allowing extraction of soil profiles along a single plane and visualisation of the progressive surface deformation.

2.4 Test procedure

Before each test, the anchor was positioned at the end of the box above the sand surface. Its initial orientation was adjusted so that the top surface of the fluke was as horizontal as possible, corresponding to zero initial roll, pitch, and yaw (Figure 1a). During installation, the vertical actuator was driven upward at a constant speed of 0.1 mm/s. Owing to the pulley arrangement, the anchor was dragged along the longitudinal (x) direction of the box at a velocity of 0.2 mm/s.

During each test, the actuator was paused at predetermined stages to allow surface scanning for photogrammetric reconstruction before dragging resumed. As the tests simulate the fully drained conditions anticipated in future centrifuge modelling, these short pauses had a negligible effect on the results. Load-cell signals, actuator displacements and the image filenames were recorded at 10 Hz, providing a basis for synchronising sensor and optical measurements.

3 RESULTS AND DISCUSSION

Two almost identical tests were conducted to assess repeatability – with the only difference being that in the second test, the anchor movement was paused eight times along the dragging path to enable detailed observation of the anchor motion and soil deformation. The following sections present the measured anchor kinematics and corresponding soil response.

3.1 6-DoF tracking of anchor installation

Figure 3 illustrates the projection of the anchor on the *x–z* plane at eight (numbered) representative stopping points in Test 2, showing the progressive rotation and penetration of the fluke as drag distance increased.

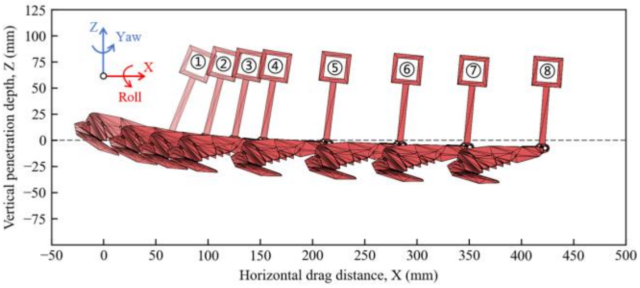

Figure 3. Anchor positions at the eight stopping points

The transformation method described in Section 2.2.2 was applied to convert the marker-tracking data to global motions of selected points on the anchor such as the padeye and fluke tip. Figure 4 presents the variation of mooring-line tension with padeye horizontal drag distance for the two tests, confirming the repeatability of the results. In the following analysis, only the results from Test 2 are discussed, and eight stopping points are marked as red dots in the figures.

Figure 5 shows the measured padeye and fluke tip penetration depths and fluke pitch angle during installation. Initially, the anchor rotated forward (positive pitch) until the padeye contacted the sand surface. It then rotated backward (negative pitch) and penetrated deeper into the sand. After Point 6, corresponding to a drag distance of approximately five fluke lengths, the anchor had almost reached an equilibrium state, with both the pitch angle and resistance becoming stable.

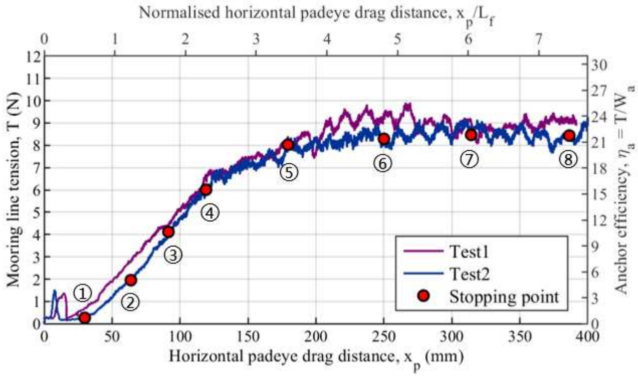

Figure 4. Development of mooring line tension with padeye drag distance

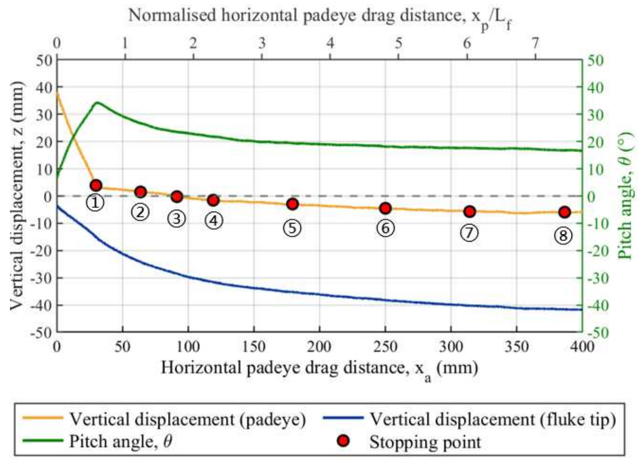

Figure 5. Vertical displacement and pitch angle vs. horizontal padeye drag distance

These results confirm that the 6-DoF marker tracking effectively captured the continuous rotation and penetration behaviour of the anchor, demonstrating that this is a reliable method for quantifying the installation kinematics for a drag anchor.

3.2 Photogrammetric reconstruction of soil deformation

Using the photogrammetric reconstructions described in Section 2.3, this section presents the evolution of soil surface deformation during anchor installation. Figure 6 presents examples of the reconstructed soil surface elevation (*z*) change in the *x*–*y* plane at four representative stages. Each reconstruction provides a detailed geometric record of the surface topography, enabling direct comparison between stages and revealing the progressive formation and widening of the trench and lateral growth of the heaved zones with drag distance. Regularly spaced shear bands were also observed on the front side of the soil heave, indicating localised shear deformation.

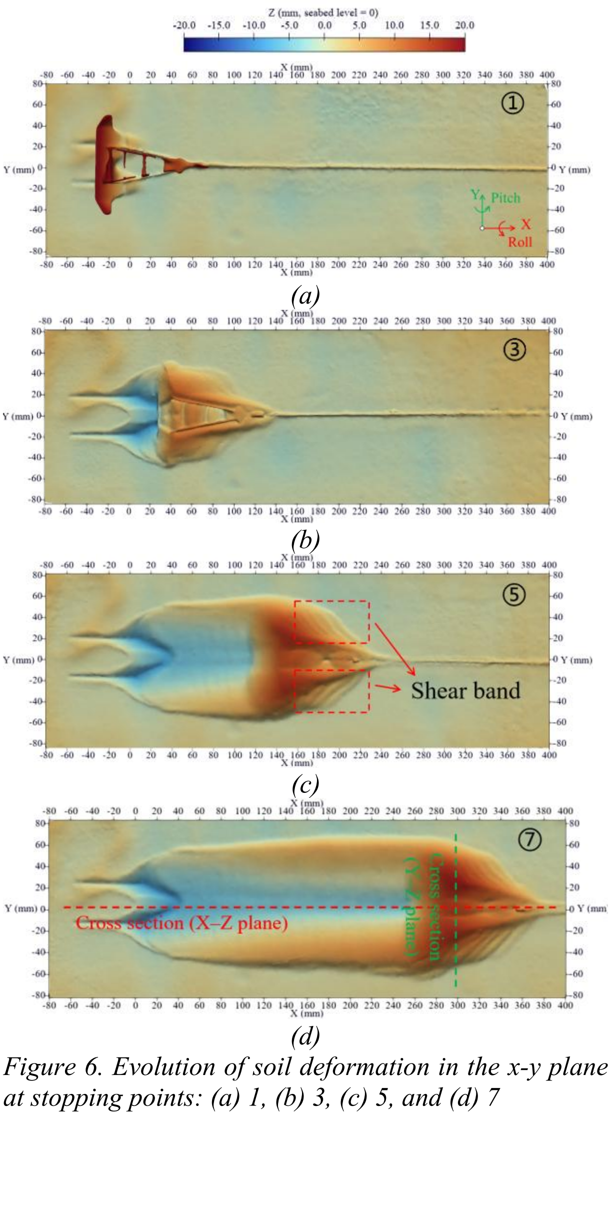

Figure 6. Evolution of soil deformation in the x-y plane at stopping points: (a) 1, (b) 3, (c) 5, and (d) 7

Cross-sectional profiles extracted from the reconstructed surfaces provide a clear visualisation of soil deformation during anchor installation. Figure 7 shows the evolution of the soil heave profile along the *x*–*z* plane (at *y* = 0 mm) at different stopping points. The soil heave exhibits an asymmetric shape – the front slope is relatively gentle due to gradual soil uplift and accumulation ahead of the fluke, whereas the rear slope is much steeper because part of the uplifted sand mass becomes unstable and collapses under its self-weight. In contrast, Figure 8 presents *y*–*z* cross-sections, which display nearly symmetrical heave shapes with steep side slopes caused by lateral spreading and local collapse of the heaved sand.

Comparison of successive reconstructions reveals two distinct stages of soil-surface development. During the early stages (Points 2 to 5), the heave expanded rapidly as the fluke displaced and lifted the surrounding sand. In the later stages (Points 6 to 8), the growth rate of the heave decreased significantly, indicating that the soil deformation had reached a relatively stable state.

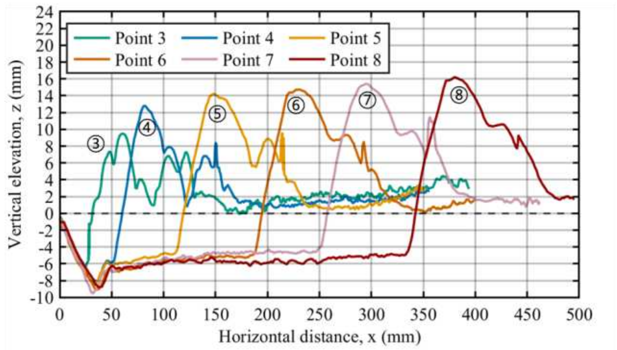

Figure 7. Soil heave profiles along the x–z plane (Y = 0 mm) at different stopping points

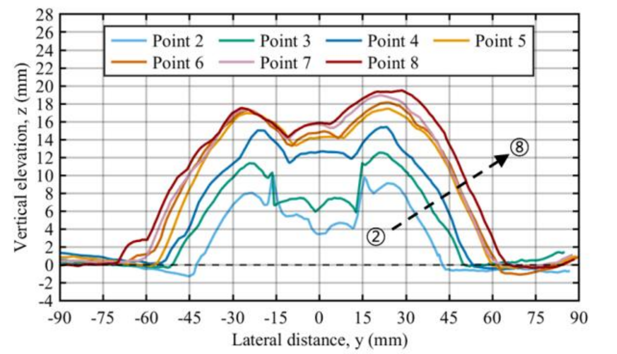

Figure 8. Soil heave profiles on the y–z plane at different stopping points

3.3 Coupled visualisation of anchor–soil interaction

This section links the measured anchor kinematics with the corresponding soil deformation during installation. Figure 9 presents an example of this combined view at the final stopping point, where the reconstructed anchor model obtained from the tracking data is superimposed on the soil heave surface reconstructed from the photogrammetry. This provides a direct spatial comparison between the anchor's configuration and the surrounding soil heave shape. In the *x*–*z* plane (Figure 9a), the inclination of the fluke top surface is comparable to the slope angle of the front soil heave, while in the *y*–*z* plane (Figure 9b), the soil heave exhibits lateral symmetry consistent with the anchor geometry.

Overall, the coupled visualisation provides clear insight into the spatial correlation between anchor movement and soil response.

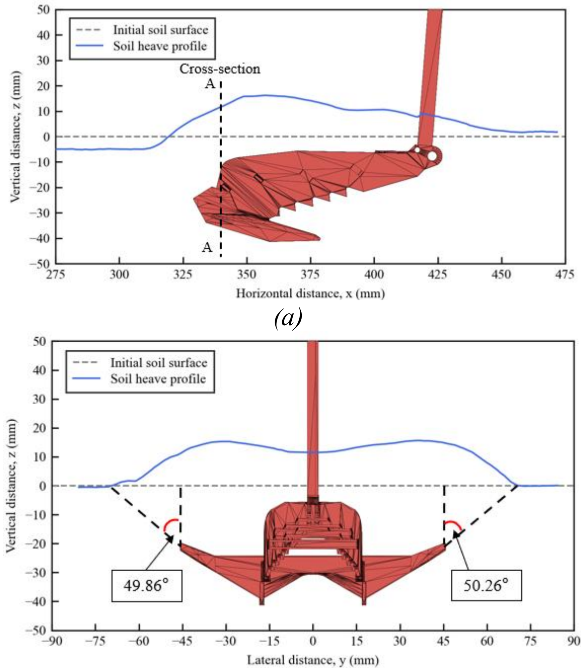

(b)

Figure 9. Coupled visualisation of anchor and soil heave profiles at the final stopping point: (a) x-z plane, (b) y-z plane (cross-section A-A)

4 CONCLUSIONS

This study demonstrates the feasibility of combining 6-DoF marker tracking and photogrammetry to investigate anchor installation in sand. The tracking system captured the anchor's rotation and penetration trajectories accurately, while the photogrammetric reconstruction provided detailed geometric representation of the evolving trench and heave features. Integration of both datasets allows direct spatial correlation between the anchor configuration and the corresponding soil deformation, providing new insight into anchor–soil interaction. The next step will be to validate this approach in the centrifuge, while the proposed system can also be extended to other geotechnical model testing, such as of pipelines, plate anchors, and piles.

ACKNOWLEDGEMENTS

The authors are grateful for the assistance from the NGCF team. This work was supported by The ARC Industrial Transformational Research Hub for Transforming energy Infrastructure through Digital Engineering (TIDE). The fourth author acknowledges the support of Fugro, provided via the Fugro Chair in Geotechnics at UWA. The fifth author leads the Shell Chair in Offshore Engineering at The University of Western Australia, which is sponsored by Shell Australia.

REFERENCES

Carchedi, D. R., Nacci, V. A., Pekin, O., & Morgan, R. J. (1984). An experimental study of drag anchors and implications for OTEC. *All Days*, OTC-4768-MS. https://doi.org/10.4043/4768-MS

Gerkus, H., Lai, Y., Senanayake, A., Gilbert, R. B., Huang, Y., Giampa, J. R., & Bradshaw, A. S. (2019). Measuring Six-Degree-of-Freedom Movements of Buried Objects in Soil Using a Magnetometer. *Geotechnical Testing Journal*, *42*(6), 1574–1586. https://doi.org/10.1520/GTJ20170328

LeLievre, B., & Tabatabaee, J. (1981). The performance of marine anchors with planar flukes in sand. *Canadian Geotechnical Journal*, *18*(4), 520–534. https://doi.org/10.1139/t81-063

Liu, H., Zhang, W., Zhang, X., & Liu, C. (2010). Experimental investigation on the penetration mechanism and kinematic behavior of drag anchors. *Applied Ocean Research*, *32*(4), 434–442. https://doi.org/10.1016/j.apor.2010.09.004

Neubecker, S. R., & Randolph, M. F. (1996). The kinematic behaviour of drag anchors in sand. *Canadian Geotechnical Journal*, *33*(4), 584–594. https://doi.org/10.1139/t96-084-306

Sharif, Y. U., Brown, M. J., Knappett, J. A., Davidson, C., Bird, R., Coombs, W., Augarde, C., Carter, G., Macdonald, C., & Johnson, K. (2025). Comparison of 1g and centrifuge modelling of drag anchors with subsurface wireless tracking. *International Journal of Physical Modelling in Geotechnics*, *25*(2), 102–114. https://doi.org/10.1680/jphmg.24.00029

Shu, S., Chen, C., Chen, H., & Lai, Y. (2022). Six-degree-of-freedom measurement of plate anchors in centrifuge by magnetometers. *China Ocean Engineering*, *36*(6), 871–879. https://doi.org/10.1007/s13344-022-0077-9

Vryhof. (2018). *Vryhof manual—Edition 8*. https://insights.delmarsystems.com/download-the-vryhof-manual